Theory and design of sound field reproduction in reverberant rooms

Terence Betlehem and Thushara D. Abhayapala[a)]
Department of Telecommunications Engineering, Research School of Information Sciences and Engineering, Australian National University, Canberra ACT 0200, Australia

(Received 19 July 2004; revised 6 January 2005; accepted 7 January 2005)

With the recent emergence of surround sound technology, renewed interest has been shown in the problem of sound field reproduction. However, in practical acoustical environments, the performance of sound reproduction techniques are significantly degraded by reverberation. In this paper, we develop a method of sound field reproduction for reverberant environments. The key to this method is an efficient parametrization of the acoustic transfer function over a region of space. Using this parametrization, a practical method has been provided for determining the transfer function between each loudspeaker and every point in the reproduction region. Through several simulation examples, the reverberant field designs have been shown to yield a reproduction accuracy as good as conventional free-field designs, and better than multipoint least squares designs when loudspeaker numbers are limited. The successful reproduction of sound over a wide frequency range has also been demonstrated. This approach reveals the appropriate choices for fundamental design parameters. [DOI: 10.1121/1.1863032]

PACS numbers: 43.60.Dh, 43.38.Md, 43.55.Br [NX] Pages: 2100–2111

I. INTRODUCTION

A problem relevant to emerging surround sound technology is a reproduction of a sound field over a region of space. Using a set of loudspeakers, it is possible for listeners to spatialize sound and fully experience what it is actually like to be in the original sound environment. Sound field reproduction has been discussed since the 1960s. However, much of the work so far does not directly address sound field reproduction in reverberant environments. In this paper, using an efficient parametrization of the room transfer function we extend sound field reproduction to reverberant enclosures.

Early work in sound field reproduction was performed by Gerzon.[1] With his ambisonics system, Gerzon reproduced the first-order spherical harmonics terms of a plane wave sound field around a point in space. Ambisonics has since been unified with holography,[2,3] both of which rely upon the Kirchoff–Helmholtz equation. Here, sound field reproduction inside a control region is achieved by controlling the pressure and its normal derivative over the boundary of the control region.[4] In similar work, global sound field reproduction techniques[5,6] have been proposed that control sound pressure over the boundary. By controlling sound at additional points inside the control region, these techniques obviate the need for velocity microphones. Unfortunately, such techniques require a large number of loudspeakers. For a lesser numbers of loudspeakers, Least squares techniques have been suggested by Kirkeby *et al.*[7,8] Recently, using spherical harmonic analysis, the theoretical minimum number of loudspeakers required for the accurate reproduction of a plane wave has been established.[9]

The reverberant case is made difficult by the rapid variation of the acoustic transfer functions over the room.[10] The standard approach has been to equalize the transfer functions over multiple points using least squares techniques.[11,12] However, in such a case, equalization can be poor away from the design points. In contrast, sound field reproduction would require the equalization to extend over the whole control region.

Alternatively, the acoustic transfer functions can be measured and incorporated into the sound field reproduction algorithm directly. Methods for estimating the acoustic transfer functions over a region have been established by Mourjopoulos[13] and Bharitkar and Kyriakakis,[14] which sample the field at a number of points and use a spatial equalization library. However, for sound field reproduction in a reverberant room, these techniques do not determine transfer functions with sufficient accuracy.

In this paper, we present a method of performing sound field reproduction in a reverberant room. This method is based on an efficient parametrization of the acoustic transfer function in the control region, where the acoustic transfer function is written as the weighted sum of a small number of orthogonal basis functions. Using this parametrization, we reconstruct a sound field accurately over the whole control region. This approach exploits the standing wave structure of the reverberant field generated by each loudspeaker to reproduce the desired sound field. We also describe a practical method for determining the acoustic transfer function between each loudspeaker and the control region, by sampling sound pressure at a small number of points.

This paper is structured as follows. In Sec. II we cast sound field reproduction into a least squares framework and introduce the basis function approach to gain insight into the fundamental parameters of the problem. In Sec. III, we describe a method of measuring the acoustic transfer functions from each speaker to any point within the control region, through measurement of the transfer function parameters of

a)Electronic mail: Thushara.Abhayapala@anu.edu.au

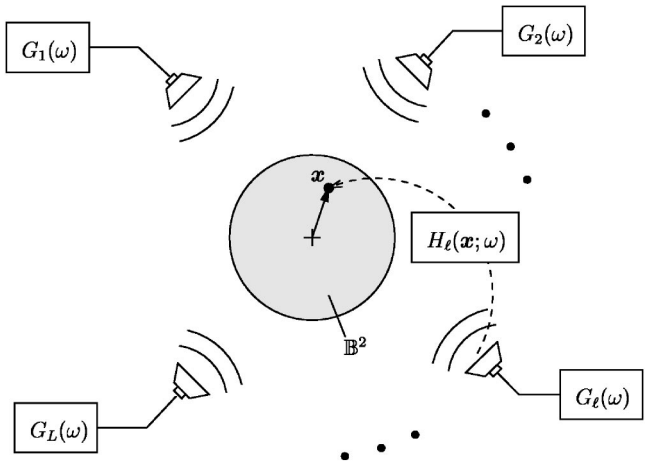

FIG. 1. Use of L loudspeakers to reproduce a desired field in a control region $\mathbb{B}^2$ with loudspeaker filters $G_l(\omega)$ and acoustical transfer functions $H_l(\mathbf{x},\omega)$ from the lth loudspeaker to a point $\mathbf{x}\in\mathbb{B}^2$.

the acoustic transfer functions. Separate methods have been derived for the narrow band and wide band cases. The effect of noisy pressure samples on measurement of the parameters has also been analyzed. Finally, in Sec. IV we demonstrate the performance of our sound field reproduction technique with several examples, including a comparison with the multiple point least squares technique.

II. SOUND FIELD REPRODUCTION

In this section, we devise a method of performing two-dimensional 2-D sound field reproduction within a reverberant enclosure. This 2-D technique ensures good reproduction in the plane of the loudspeakers, provided each loudspeaker possesses a sizable vertical dimension. It is applicable to enclosures with highly sound-absorbing floors and ceilings.

The theory we develop in this paper is readily extended to 3-D space. The 2-D basis functions that are described below need only be replaced with 3-D basis functions. Unfortunately, in the case 3-D of reproduction over a volume, much larger numbers of speakers are required.[9] We focus on reproduction in the plane as it is more practical.

Below we formulate the problem in the frequency domain. The objective is to determine the loudspeaker filter weights required to reproduce a desired sound field in a reverberant room.

A. Problem definition

We aim to reproduce the pressure $P_d(\mathbf{x};\omega)$ of a desired sound field at each point $\mathbf{x}$ and angular frequency ω in the source-free region of interest $\mathbb{B}^2$ using an array of L loudspeakers. The desired sound field could be a plane wave, a field resulting from a monopole, a field measured in a real-life scenario or the field of a surround sound system. For purposes of simplifying the analysis in this paper, we choose the control region $\mathbb{B}^2$ to be the circle of radius R centered about the origin:

$$\mathbb{B}^2=\{\mathbf{x}\in\mathbb{R}^2:\|\mathbf{x}\|\leqslant R\},$$

where $\|\cdot\|$ denotes the Euclidean distance.

As shown in Fig. 1, each loudspeaker l transmits an output signal $G_l(\omega)$. This signal encapsulates both the input signal applied to loudspeaker l as well as any filtering of it. To characterize the acoustic properties of the enclosure, define the acoustic transfer function $H_l(\mathbf{x};\omega)$ as the frequency response between loudspeaker l and point $\mathbf{x}$. $H_l(\mathbf{x};\omega)$ summarizes the effect of reverberant reflections from the surface of the enclosure on any sound signal transmitted by each loudspeaker. The sound pressure at any point $\mathbf{x}$ due to loudspeaker l is equal to

$$P_l(\mathbf{x};\omega)=G_l(\omega)H_l(\mathbf{x};\omega). \tag{1}$$

From Fig. 1, the sound pressure in the reproduced field resulting from the L loudspeakers is then equal to

$$P(\mathbf{x};\omega)=\sum_{l=1}^{L} P_l(\mathbf{x};\omega)=\sum_{l=1}^{L} G_l(\omega)H_l(\mathbf{x};\omega). \tag{2}$$

The design task of sound field reproduction is to choose filter weights $G_l(\omega)$ to minimize the normalized reproduction error $\mathcal{T}$ over $\mathbb{B}^2$,

$$\mathcal{T}=\frac{1}{\mathcal{E}}\int_{\mathbb{B}^2}|P(\mathbf{x};\omega)-P_d(\mathbf{x};\omega)|^2\,da(\mathbf{x}), \tag{3}$$

where the normalizing factor $\mathcal{E}$ is the energy of the desired sound field over $\mathbb{B}^2$:

$$\mathcal{E}=\int_{\mathbb{B}^2}|P_d(\mathbf{x};\omega)|^2\,da(\mathbf{x}), \tag{4}$$

$da(\mathbf{x})=x\,dx\,d\phi_x$ is the differential area element at $\mathbf{x}$, $x=\|\mathbf{x}\|$, and ϕ_x is the polar angle of $\mathbf{x}$.

The popular approach to solving this problem is to write the least squares solution over a set of uniformly spaced points over $\mathbb{B}^2$. (Refs. 7, 8). A better approach is to perform the design over the whole region. This approach is proposed by Asano and Swason[15] for the related problem of equalization. Yet by discretizing, these authors end up implementing a multipoint method. Below we outline a model-based approach, which uses an efficient parametrization for acoustic transfer functions to perform the design over the whole region. This model-based approach is more general than the approach of Asano and Swason[15] and Santillan,[16] which assume that the room is of a rectangular shape. More insight is gained into the design requirements for an accurate reproduction through the model-based approach than through multipoint least squares techniques.

B. Model-based approach

In the model-based approach, we express the sound pressure variables $P_d(\mathbf{x};\omega)$, $P(\mathbf{x};\omega)$, and the acoustic transfer functions $H_l(\mathbf{x};\omega)$ in terms of the basis functions of the sound field. Provided all sound sources (including image sources produced by reflection) lie outside of $\mathbb{B}^2$, at any point inside $\mathbb{B}^2$ the above variables can be written as a weighted sum of the inward-propagating solutions to the wave equation.[17] We write the desired sound pressure $P_d(\mathbf{x};\omega)$ as

$$P_d(\mathbf{x};\omega)=\sum_{n=-\infty}^{\infty}\beta_n^{(d)}(\omega)J_n(kx)e^{in\phi_x}, \tag{5}$$

where $\beta_n^{(d)}(\omega)$ is the nth-order sound field coefficient of the desired sound field, $J_n(\cdot)$ is the Bessel function of order n and $k=\omega/c=2\pi/\lambda$ is the wave number, c is the speed of sound in air, and λ is the acoustic wavelength. The functions $\{J_n(kx)e^{in\phi_x}\}_{n\in\mathbb{Z}}$ are called the basis functions of the sound field. An appropriate choice of sound field coefficients generate any valid sound field inside $\mathbb{B}^2$.

Similarly, we write the reproduced sound pressure $P(\mathbf{x};\omega)$ as

$$P(\mathbf{x};\omega)=\sum_{n=-\infty}^{\infty}\beta_n(\omega)J_n(kx)e^{in\phi_x}, \tag{6}$$

where $\beta_n(\omega)$ are the coefficients of the reproduced sound field. A reproduction of the sound pressure $P_d(\mathbf{x};\omega)$ over $\mathbb{B}^2$ with $P(\mathbf{x};\omega)$ is equivalent to a reproduction of the sound field coefficients $\{\beta_n^{(d)}(\omega)\}_{n\in\mathbb{Z}}$ with $\{\beta_n(\omega)\}_{n\in\mathbb{Z}}$.

Because the room response is equal to the sound field pressure generated by the unit input signal $G_l(\omega)$, we can also write it as

$$H_l(\mathbf{x};\omega)=\sum_{n=-\infty}^{\infty}\alpha_n(l,\omega)J_n(kx)e^{in\phi_x}, \tag{7}$$

where $\alpha_n(l,\omega)$ are the sound field coefficients of the room responses for loudspeaker l. These sound field coefficients completely characterize the reverberant sound field generated by each loudspeaker within $\mathbb{B}^2$:

Observation 1: *When the sound field coefficients $\alpha_n(l,\omega)$ for each loudspeaker are known for a given room, the acoustic transfer function $H_l(\mathbf{x};\omega)$ between each loudspeaker and any position $\mathbf{x}$ inside $\mathbb{B}^2$ is also known, and is given by Eq. (7).*

Substituting Eq. (5) and Eq. (7) directly into Eq. (2), the coefficients of the reproduced sound field are related to $\alpha_n(l,\omega)$ through

$$\beta_n(\omega)=\sum_{l=1}^{L}G_l(\omega)\alpha_n(l,\omega). \tag{8}$$

The sequences of coefficients $[\beta_n^{(d)}(\omega))_n$, $(\beta_n(\omega))_n$ and $(\alpha_n(l,\omega)]$ associated with any wave field in a source-free region are shown to be bounded.[18] (These coefficients are bounded in the following sense. Any field in the source-free region can be represented as the superposition of plane waves. The coefficients are bounded by the sum of the magnitudes of these plane waves.)

A benefit of the model-based approach is the ability to express key variables in terms of orthogonal functions. Using the orthogonality property of exponential functions,

$$\int_0^{2\pi}e^{-in\phi}e^{im\phi}\,d\phi=2\pi\delta_{nm}, \tag{9}$$

we derive an expression for the energy $\mathcal{E}$ and normalized error $\mathcal{T}$ of the reproduced sound field over $\mathbb{B}^2$ as a function of the sound field coefficients. Starting with the field energy, we substitute Eq. (5) into Eq. (4) to yield

$$\mathcal{E}=\int_{\mathbb{B}^2}\left|\sum_{n=-\infty}^{\infty}\beta_n^{(d)}(\omega)J_n(kx)e^{in\phi_x}\right|^2 da(\mathbf{x}).$$

It follows that

$$\begin{aligned}\mathcal{E}&=\int_{\mathbb{B}^2}\sum_{n_1=-\infty}^{\infty}[\beta_{n_1}^{(d)}(\omega)]^*J_{n_1}(kx)e^{-in_1\phi_x}\\&\quad\times\sum_{n_2=-\infty}^{\infty}\beta_{n_2}^{(d)}(\omega)J_{n_2}(kx)e^{in_2\phi_x}\,da(\mathbf{x})\\&=\sum_{n_1=-\infty}^{\infty}\sum_{n_2=-\infty}^{\infty}[\beta_{n_1}^{(d)}(\omega)]^*\beta_{n_2}^{(d)}(\omega)\\&\quad\times\int_0^{2\pi}e^{-in_1\phi_x}e^{in_2\phi_x}\,d\phi_x\\&\quad\times\int_0^{R}J_{n_1}(kx)J_{n_2}(kx)x\,dx,\end{aligned}$$

where we have applied $da(\mathbf{x})=x\,dx\,d\phi_x$ in the second step. Applying the orthogonality property, Eq. (9), of the exponential functions, the field energy reduces to

$$\begin{aligned}\mathcal{E}&=2\pi\sum_{n=-\infty}^{\infty}|\beta_n^{(d)}(\omega)|^2\int_0^R[J_n(kx)]^2x\,dx\\&=K\sum_{n=-\infty}^{\infty}w_n(kR)|\beta_n^{(d)}(\omega)|^2,\end{aligned} \tag{10}$$

where $K=2\pi/k^2$ and

$$w_n(kR)\triangleq k^2\int_0^R[J_n(kx)]^2x\,dx=\int_0^{kR}[J_n(x)]^2x\,dx. \tag{11}$$

The second step was performed with the variable substitution $x'=kx$. Similarly, substituting Eq. (5) and Eq. (6) into Eq. (3), the normalized error becomes

$$\mathcal{T}=\frac{1}{\mathcal{E}}\int_{\mathbb{B}^2}\left|\sum_{n=-\infty}^{\infty}[\beta_n^{(d)}(\omega)-\beta_n(\omega)]J_n(kx)e^{in\phi_x}\right|^2 da(\mathbf{x}).$$

Utilizing the orthogonality property, the normalized error reduces to

$$\mathcal{T}=\frac{K}{\mathcal{E}}\sum_{n=-\infty}^{\infty}w_n(kR)|\beta_n^{(d)}(\omega)-\beta_n(\omega)|^2. \tag{12}$$

We shall call $w_n(kR)$ in (12) the *coefficient weighting function*.

Since the summations in Eq. (5), Eq. (6), and Eq. (7) have infinite numbers of terms, it may seem that the above parametrizations need an infinite number of coefficients. However, in the next section, we show that for any finite control region, they need only a finite number of coefficients to accurately represent a sound field or a room response.

C. Active basis functions

Because of the high-pass character of Bessel functions, not all of the basis functions make a significant energy contribution to the sound field inside $\mathbb{B}^2$. Studying Eq. (12), because the sequences of sound field coefficients $[\beta_n^{(d)}(\omega)]_n$ and $[\beta_n(\omega)]_n$ are bounded while from Fig. 2,

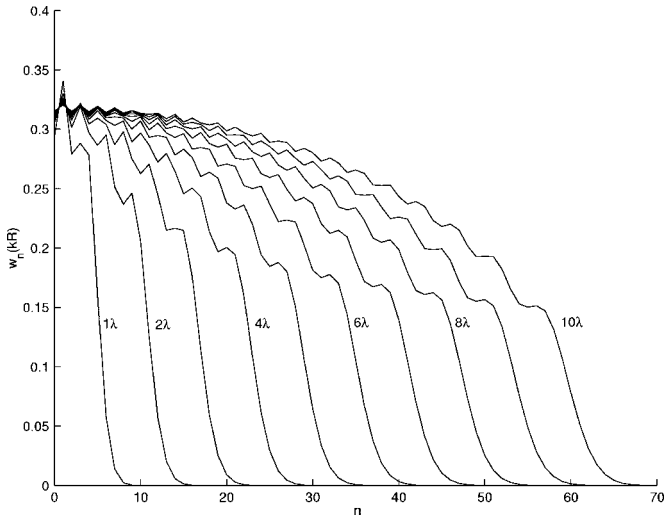

FIG. 2. A plot of the coefficient weighting function $w_{|n|}(kR)$ vs $|n|$ for control regions with radii $R=[1\lambda,2\lambda,\ldots,10\lambda]$. λ is the acoustic wavelength of interest, related to the wave number by $k=2\pi/\lambda$.

$w_n(kR)$ drop rapidly to zero past a threshold, the energy contribution of each term to reproduction error is controlled by $w_n(kR)$.

Previous work[9,18] asserts that only the basis functions of index up to $N=\lceil kR \rceil$ contribute significant energy to the sound field inside $\mathbb{B}^2$. This result is supported by Fig. 2, where $w_{|n|}(kR)$ is plotted against $|n|$. [Note the coefficient weighting functions of negative index are a mirror of those of positive index $w_{-n}(kR)=w_n(kR)$. This can be seen by applying the Bessel function property $J_n(x)=(-1)^n J_{-n}(x)$.] The weighting is seen to be small past $|n|>N$. The $2N+1$ basis functions, $J_{-N}(kx)e^{-iN\phi_x},\ldots,J_N(kx)e^{iN\phi_x}$ are referred to as *active* in $\mathbb{B}^2$. The remaining basis functions are referred to as *inactive* in $\mathbb{B}^2$. Such basis functions only contribute significant energy to the sound field outside of $\mathbb{B}^2$.

An accurate sound field reproduction requires the reproduction of these active basis functions. Also, the acoustic transfer functions mentioned in Observation 1 are accurately determined just by measuring the sound field coefficients $\{\alpha_n(l,\omega)\}_{n=-N}^{N}$ of the active basis functions.

D. Least squares solution

We now derive the least squares solution for the speaker filter weights that minimizes the reproduction error in Eq. (12). This solution is expressed in terms of the sound field coefficients.

Because the weighting of terms in the normalized error in Eq. (12) rapidly diminish for $|n|\geqslant N$, it can be truncated to

$$\mathcal{T}_{N_T}=\frac{K}{\mathcal{E}}\sum_{n=-N_T}^{N_T} w_n(kR)\left|\beta_n(\omega)-\beta_n^{(d)}(\omega)\right|^2, \tag{13}$$

for $N_T\geqslant N$. This truncated reproduction error $\mathcal{T}_{N_T}$ can be written in matrix form, as follows. Defining the vector of loudspeaker filter weights $\mathbf{g}=[G_1(\omega),G_2(\omega),\ldots,G_L(\omega)]^T$, where $[\cdot]^T$ is the matrix transpose operator, the vector of the coefficients of the reproduced sound field $\boldsymbol{\beta}=[\beta_{-N_T}(\omega),\beta_{-N_T+1}(\omega),\ldots,\beta_{N_T}(\omega)]^T$, and the matrix of the coefficients of the room responses of all loudspeakers,

$$\mathbf{A}=\begin{bmatrix} \alpha_{-N_T}(1,\omega) & \alpha_{-N_T}(2,\omega) & \cdots & \alpha_{-N_T}(L,\omega) \\ \alpha_{1-N_T}(1,\omega) & \alpha_{1-N_T}(2,\omega) & \cdots & \alpha_{1-N_T}(L,\omega) \\ \vdots & \vdots & \ddots & \vdots \\ \alpha_{N_T}(1,\omega) & \alpha_{N_T}(2,\omega) & \cdots & \alpha_{N_T}(L,\omega) \end{bmatrix}, \tag{14}$$

Eq. (8) can be rewritten as $\boldsymbol{\beta}=\mathbf{A}\mathbf{g}$. Additionally, define the vectors of the coefficients of the desired sound field, $\boldsymbol{\beta}_d=[\beta_{-N_T}^{(d)}(\omega),\beta_{-N_T+1}^{(d)}(\omega),\ldots,\beta_{N_T}^{(d)}(\omega)]^T$, and the diagonal weighting matrix,

$$\mathbf{W}=\begin{bmatrix} w_{-N_T}(kR) & 0 & \cdots & 0 \\ 0 & w_{-N_T+1}(kR) & \cdots & 0 \\ \vdots & \vdots & \ddots & \vdots \\ 0 & 0 & \cdots & w_{N_T}(kR) \end{bmatrix}.$$

Writing the numerator of Eq. (13) in matrix form:

$$\sum_{n=-N_T}^{N_T} w_n(kR)\left|\beta_n(\omega)-\beta_n^{(d)}(\omega)\right|^2=(\boldsymbol{\beta}-\boldsymbol{\beta}_d)^{\mathrm{H}}\mathbf{W}(\boldsymbol{\beta}-\boldsymbol{\beta}_d),$$

where $(\cdot)^{\mathrm{H}}$ is the matrix Hermitian operator, the truncated reproduction error can be written as

$$\mathcal{T}_{N_T}=\frac{(\boldsymbol{\beta}-\boldsymbol{\beta}_d)^{\mathrm{H}}\mathbf{W}(\boldsymbol{\beta}-\boldsymbol{\beta}_d)}{\boldsymbol{\beta}_d^{\mathrm{H}}\mathbf{W}\boldsymbol{\beta}_d}.$$

Since $\boldsymbol{\beta}=\mathbf{A}\mathbf{g}$, we expand the truncated reproduction error as a quadratic form in the vector of loudspeaker filter weights:

$$\mathcal{T}_{N_T}(\mathbf{g})=\frac{1}{d}(\mathbf{g}^{\mathrm{H}}\mathbf{B}\mathbf{g}-\mathbf{b}^{\mathrm{H}}\mathbf{g}-\mathbf{g}^{\mathrm{H}}\mathbf{b}+d),$$

where $\mathbf{B}=\mathbf{A}^{\mathrm{H}}\mathbf{W}\mathbf{A}$, $\mathbf{b}=\mathbf{A}^{\mathrm{H}}\mathbf{W}\boldsymbol{\beta}_d$, $d=\boldsymbol{\beta}_d^{\mathrm{H}}\mathbf{W}\boldsymbol{\beta}_d$. This quadratic form possesses it's global minimum at[15]

$$\hat{\mathbf{g}}=\mathbf{B}^{-1}\mathbf{b}=(\mathbf{A}^{\mathrm{H}}\mathbf{W}\mathbf{A})^{-1}\mathbf{A}^{\mathrm{H}}\mathbf{W}\boldsymbol{\beta}_d, \tag{15}$$

with the associated minimum in truncated reproduction error:

$$\mathcal{T}_{N_T}(\hat{\mathbf{g}})=1-\frac{1}{d}\mathbf{b}^{\mathrm{H}}\mathbf{B}^{-1}\mathbf{b}.$$

Once $(\mathbf{A}^{\mathrm{H}}\mathbf{W}\mathbf{A})^{-1}\mathbf{A}^{\mathrm{H}}\mathbf{W}$ is computed for the acoustical environment, the reproduced sound field can be changed easily by modifying $\boldsymbol{\beta}_d$.

E. Multiple-point approach

For comparison, we describe the conventional least squares approach, where the sound field is reproduced at several points. Here we aim to reproduce the desired sound field $P_d(\mathbf{x};\omega)$ over M points $\mathbf{x}_1$, $\mathbf{x}_2,\ldots,\mathbf{x}_M$, positioned within the region of interest $\mathbb{B}^2$ with $M\geqslant L$. Define the vector of desired sound pressure at each point $\mathbf{p}_d=[P_d(\mathbf{x}_1;\omega),P_d(\mathbf{x}_2;\omega),\ldots,P_d(\mathbf{x}_M;\omega)]^T$, and the acoustic transfer functions between the loudspeakers and control points into the matrix,

$$\mathbf{H}=\begin{bmatrix} H_1(\mathbf{x}_1;\omega) & H_2(\mathbf{x}_1;\omega) & \cdots & H_L(\mathbf{x}_1;\omega) \\ H_1(\mathbf{x}_2;\omega) & H_2(\mathbf{x}_2;\omega) & \cdots & H_L(\mathbf{x}_2;\omega) \\ \vdots & \vdots & \ddots & \vdots \\ H_1(\mathbf{x}_M;\omega) & H_2(\mathbf{x}_M;\omega) & \cdots & H_L(\mathbf{x}_M;\omega) \end{bmatrix}.$$

The loudspeaker weights are determined from the (possibly overdetermined) system $\mathbf{Hg}=\mathbf{p}$. The least squares solution is then given by $\hat{\mathbf{g}}=\mathbf{H}^{\dagger}\mathbf{p}$, where $[\cdot]^{\dagger}$ is the Moore–Penrose inverse.

In Sec. IV, the multiple-point approach has been compared to the model-based approach. We shall see that since the model-based approach targets reproduction over the whole control region, it yields superior performance to the multiple-point approach.

In the next section we describe a method for measuring coefficients for the acoustic transfer function in matrix $\mathbf{A}$ for the model-based approach.

III. ESTIMATION OF SOUND FIELD COEFFICIENTS

In this section we describe how to fully determine the sound field inside a control region $\mathbb{B}^2$ through measurement of the sound field coefficients. This task is important as it is required to calculate $\{\alpha_n(l,\omega)\}_{n\in\mathbb{Z}}$ that characterize the reverberant field generated by each loudspeaker.

We write the sound pressure $P(\mathbf{x};\omega)$ inside $\mathbb{B}^2$ generated by a loudspeaker outside $\mathbb{B}^2$ in a reverberant enclosure as the basis function expansion:

$$P(\mathbf{x};\omega)=\sum_{n=-\infty}^{\infty}\beta_n(\omega)J_n(kx)e^{in\phi_x}, \tag{16}$$

where $\beta_n(\omega)$ is the sound field coefficient of order n. To determine the field pressure inside $\mathbb{B}^2$, we describe a simple means of measuring $\beta_n(\omega)$.

The method used to determine the sound field coefficients varies depending on whether they are required in a narrow range of frequencies (Sec. III A) or a wide range of frequencies (Sec. III B).

A. Narrow-band method

In the case that sound field reproduction is performed in a narrow frequency range for a choice of R, away from any zero of $J_n(kR)$, good sound field coefficient estimates are obtained by sampling pressure over a single circle of radius R.

1. Computation of sound field coefficients

The sound field coefficients are obtained from the analysis equation,

$$\beta_n(\omega)=\frac{1}{2\pi J_n(kx)}\int_0^{2\pi}P(\mathbf{x};\omega)e^{-in\phi_x}\,d\phi_x, \tag{17}$$

provided x is not a zero of $J_n(kx)$. This equation is derived by multiplying both sides of Eq. (16) by $e^{-in'\phi}$, integrating, and applying the orthogonality property. Interpreting this equation, the sound field coefficients and hence sound field can be known in the whole of $\mathbb{B}^2$ just by measuring sound pressure on a circle of radius x.

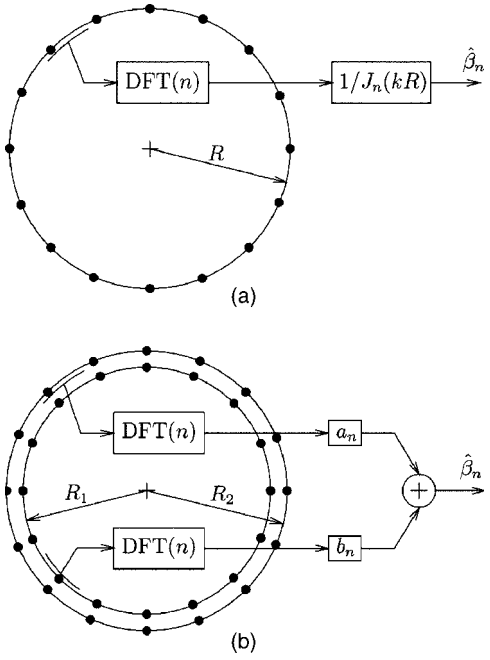

FIG. 3. Proposed methods for measuring the sound field coefficients $\hat{\beta}_n(\omega)$ in (a) the narrow band case where pressure is sampled at one radius R and (b) the wide band case where pressure is sampled at two radii, R_1 and R_2.

In this paper we sample pressure at $x=R$, on the boundary of $\mathbb{B}^2$. Now at a radius x, only basis functions of order up to $\lceil kx \rceil$ are active. Over the boundary all of the active basis functions of $\mathbb{B}^2$ are active, while the higher-order basis functions are inactive. So heuristically this choice of sampling radius makes sense.

Approximate sound field coefficients $\hat{\beta}_n(\omega)$ are obtained by sampling sound pressure at M evenly spaced points (R,ϕ_m), where $\phi_m=2\pi m/M$ for $m=0,1,...,M-1$. Since Eq. (17) shows $\beta_n(\omega)J_n(kR)$ are the Fourier series coefficients of $P(R,\phi;\omega)$ in variable ϕ. Consequently, it can be approximated with the discrete Fourier transform (DFT) relationship:

$$\hat{\beta}_n(\omega)=\frac{1}{J_n(kR)}\mathrm{DFT}\{P(R,\phi_m;\omega)\}(n), \tag{18}$$

where $\mathrm{DFT}\{f(m)\}(n)$ is the M-point DFT, defined by

$$\mathrm{DFT}\{f(m)\}(n)=\frac{1}{M}\sum_{m=0}^{M-1}f(m)e^{-i(2\pi mn/M)}. \tag{19}$$

Coefficients $\hat{\beta}_n(\omega)$ are recognized as the DFT of the sampled field pressure around the circle $\{P(R,2\pi m/M;\omega)\}_{m=0}^{M-1}$, weighted by the Bessel function term $1/J_n(kR)$ [Fig. 3(a)].

An appropriate choice for M can be deduced by noting that the sound field in $\mathbb{B}^2$ is the result of $2N+1$ active basis functions. Since one equation is required for each sound field coefficient, we need at least $M=2N+1$ pressure samples where $N=\lceil kR \rceil$.

Due to the presence of $1/J_n(kR)$ in Eq. (18), if kR is near one of the Bessel zeros, coefficient error is amplified. This error amplification can be negated by oversampling pressure, as is seen in the next section.

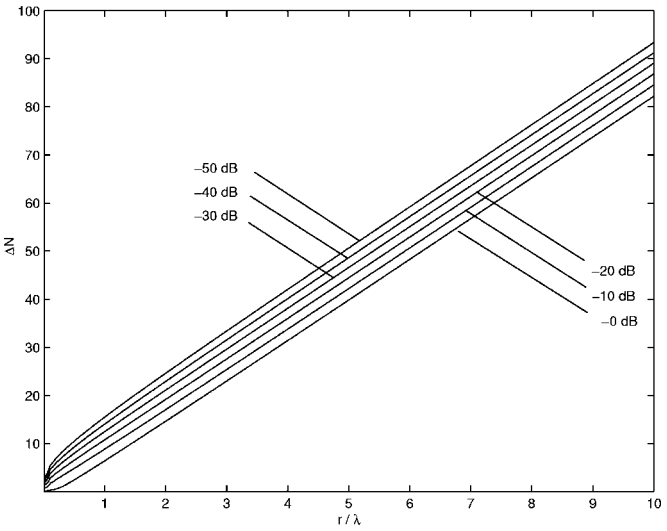

FIG. 4. Sample measurement parameter ΔN required for several values of ϵ' (in dB). The curves show the ΔN required to ensure that $|J_{\Delta N}(kR)|$ is upper bounded by ϵ'. The total number of pressure samples required is then $N+\lceil\Delta N\rceil$, where N is the number of active basis functions.

2. Approximation error

In Appendix A, we show the error in the approximated sound field coefficients $\hat{\beta}(\omega)$ is given by

$$\hat{\beta}_n(\omega)-\beta_n(\omega)=\frac{1}{J_n(kR)}\sum_{q=-\infty,\neq 0}^{\infty} J_{n+qM}(kR)\beta_{n+qM}(\omega). \tag{20}$$

This equation reveals a type of aliasing, since the higher-order coefficients $\{\beta_{n+qM}(\omega)\}_{q=-\infty,\neq 0}^{\infty}$ are mapped onto each $\hat{\beta}_n(\omega)$. It also shows the magnitude of the approximation error is controlled by the size of $1/J_n(kR)$. We shall refer to the summation term in Eq. (20) as the *aliasing error* and the preceding $1/J_n(kR)$ term as the *error scaling*. If $J_n(kR)$ is small, the error scaling is large.

From Eq. (20), each basis function of index $n+qM$ makes a termwise contribution of $[J_{n+qM}(kR)/J_n(kR)]\beta_{n+qM}(\omega)$ for $q\neq 0$ to the approximation error in $\hat{\beta}_n(\omega)$. We now identify a choice of M that ensures the termwise scale factor $J_{n+qM}(kR)/J_n(kR)$ arbitrarily small.

Define κ_n as the largest *termwise scale factor* in $\beta_n(\omega)$:

$$\kappa_n \triangleq \max_{q=-\infty,\ldots,\infty,\neq 0}\left|\frac{J_{n+qM}(kR)}{J_n(kR)}\right|, \tag{21}$$

for $n=-N,-N+1,\ldots,N$. In Appendix B, the largest termwise scale factor of all of the active basis functions is shown to be bounded by

$$\max_{n=-N,\ldots,N}\kappa_n \leqslant \underbrace{\max_{n=0,\ldots,N} 1/|J_n(kR)|}_{\kappa_{\mathrm{es}}} \times \underbrace{\frac{1}{\sqrt{2\pi(M-N)}}\left[\frac{ekR}{2(M-N)}\right]^{M-N}}_{\text{upper bound on } |J_{M-N}(kR)|}. \tag{22}$$

The first term in this bound is the maximum error scaling that we shall denote as κ_{es}. The second term is a bound on the Bessel function $J_{M-N}(kR)$ obtained from Jones *et al.*[18] We note in Eq. (22) that the largest termwise scaling factor decays exponentially to zero as M is increased past $N+\lceil ekR/2\rceil$. This observation suggests choosing $M\approx N+\lceil ekR/2\rceil$. However, a better procedure for the choice of M, motivated by the form of Eq. (22) is presented next.

3. Conservative estimate of M

This procedure allows a more accurate choice of M.

(a) Choose the desired bound ϵ on the termwise scale factor; i.e., choose a bound for which $\max_{n=-N,\ldots,N}\kappa_n<\epsilon$.

(b) Calculate the maximum error scaling: $\kappa_{\mathrm{es}}=\max_{n=0,1,\ldots,N}|1/J_n(kR)|$.

(c) Determine $\Delta N=M-N$ to guarantee $|J_{N-M}(kR)|$ is upper bounded by $\epsilon'=\epsilon/\kappa_{\mathrm{es}}$ through the relationship

$$\frac{1}{\sqrt{2\pi\,\Delta N}}\left[\frac{ekR}{2\,\Delta N}\right]^{\Delta N}=\epsilon'. \tag{23}$$

Equation (23) has been plotted in Fig. 4 for several values of ϵ'.

(d) The required number of samples $M=N+\lceil\Delta N\rceil$.

A judicious choice of radius R ensures that κ_{es} is minimal. Further, such a choice will result in minimizing the number of required pressure samples.

Interestingly, Fig. 4 shows a linear relationship between ΔN and kR for large kR. Rearranging Eq. (23):

$$\Delta N=\frac{e}{2}(\sqrt{2\pi\Delta N}\epsilon')^{-1/\Delta N}kR.$$

As $\Delta N\to\infty$, the term $(\sqrt{2\pi\,\Delta N}\epsilon')^{-1/\Delta N}\to 1$, causing this expression to reduce to $\Delta N\approx ekR/2$. This relationship explains the linear section of the curves in Fig. 4 and is consistent with the $N+\lceil ekR/2\rceil$ rule.

In summary, we require at least $M=2N+1$ pressure samples to measure the sound field coefficients of the active basis functions. An analysis of the error in approximated sound field coefficients shows that for an accurate measurement of sound field coefficients more pressure samples may be required. The larger M is required to negate the effects of error scaling. A conservative procedure for estimating M is summarized above.

B. Wide band method

In frequency ranges and sizes of $\mathbb{B}^2$ of interest to practical problems, the Bessel term $J_n(kR)$ is guaranteed to be zero at a number of frequencies. These zeros cause problems when designing with the above method over a wide frequency range. For each zero, a basis functions remains unmeasurable.

To illustrate the magnitude of the problem, consider the asymptotic behavior (that is, the behavior for large kR) of the Bessel function:[17]

$$J_n(kR)\sim\sqrt{\frac{2}{\pi kR}}\cos(kR-n\pi/2-\pi/4). \tag{24}$$

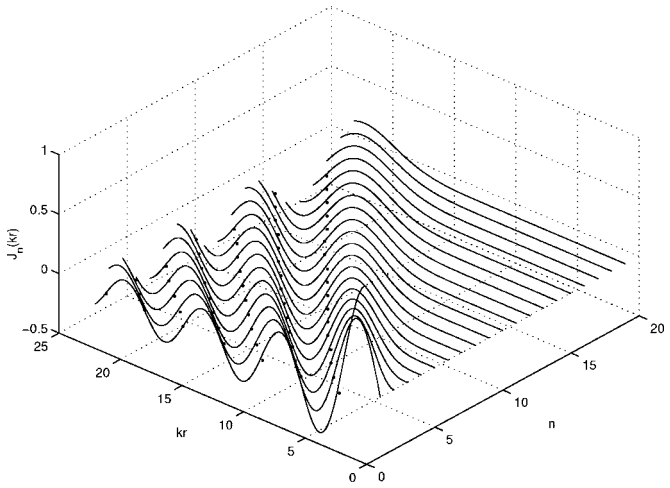

FIG. 5. Bessel functions $J_n(kR)$ that are active in a control region of radius 0.3 m and frequencies up to 4 kHz. Each zero of the Bessel functions is marked with a dot $(\cdot)$.

One can see from this equation that each of the Bessel functions has zeros spaced approximately $kR=\pi$ or $f=c/2R$ apart. In a region $\mathbb{B}^2$ with radius $R=0.3\,\mathrm{m}$ and speed of sound $c=342\,\mathrm{m/s}$, each $J_n(kR)$ has zeros spaced 570 Hz apart. In a 0–4 kHz frequency range there are 58 zeros present (Fig. 5). On average, one zero occurs every 69 Hz, with the larger concentration of zeros at higher frequencies.

To combat this problem, we propose an alternative method for the wide-band case. Instead of sampling over a single radius R we sample over two concentric circles of radii $R_1=R-\delta R$ and $R_2=R$ [Fig. 3(b)].

1. Computation of sound field coefficients

Multiplying both sides of Eq. (16) by basis function $J_{n'}(kx)e^{-in'\phi_x}$ and integrating over the thin shell of thickness $\delta R=R_2-R_1$, $\{\mathbf{x}\in\mathbb{R}^2:R_1\leqslant\|\mathbf{x}\|\leqslant R_2\}$, the orthogonality property, Eq. (9), is used to show that

$$\beta_n(\omega)=\frac{1}{2\pi\int_{R_1}^{R_2}[J_n(kx)]^2x\,dx}\times\int_{R_1}^{R_2}\int_0^{2\pi}P(\mathbf{x};\omega)J_n(kx)e^{-in\phi_x}x\,dx\,d\phi_x.$$

For small δR, we can approximate the integral in x with the zeroth-order approximation:

$$\int_{R_1}^{R_2}f(x)dx=\frac{1}{2}[f(R_1)+f(R_2)]\delta R. \tag{25}$$

Using Eq. (25), we express $\beta_n(\omega)$ as a sum of two weighted Fourier series equations. Sampling the field with M evenly spaced sensor pairs positioned at (R_1,ϕ_m) and (R_2,ϕ_m), the sound field coefficients $\beta_n(\omega)$ are estimated with

$$\hat{\beta}_n(\omega)=a_n(\omega)\mathrm{DFT}\{P(R_1,\phi_m;\omega)\}(n)+b_n(\omega)\mathrm{DFT}\{P(R_2,\phi_m;\omega)\}(n), \tag{26}$$

where for $R_1\approx R_2$, the DFTs are weighted by

$$a_n(\omega)=\frac{J_n(kR_1)}{[J_n(kR_1)]^2+[J_n(kR_2)]^2}, \tag{27}$$

$$b_n(\omega)=\frac{J_n(kR_2)}{[J_n(kR_1)]^2+[J_n(kR_2)]^2}. \tag{28}$$

The approximated sound field coefficients can hence be obtained through taking the DFT of the pressure samples around each circle and calculating a weighted average.

Next we analyze the error in the approximated sound field coefficients.

2. Approximation error

For the wide band method, the error in the approximated sound field coefficients is

$$\hat{\beta}_n(\omega)-\beta_n(\omega)=a_n(\omega)\sum_{q=-\infty,\neq 0}^{\infty}J_{n+qM}(kR_1)\beta_{n+qM}(\omega)+b_n(\omega)\sum_{q=-\infty,\neq 0}^{\infty}J_{n+qM}(kR_2)\beta_{n+qM}(\omega). \tag{29}$$

This expression is proven by substituting Eq. (19) into Eq. (26) and simplifying the resulting expression in a manner similar to that in Appendix A. In contrast to the narrow band case in Eq. (20), the wide band case possesses two error scaling terms, $a_n(\omega)$ and $b_n(\omega)$. Also, the presence of $[J_n(kR_1)]^2+[J_n(kR_2)]^2$ in the denominators of the error scaling terms [see Eq. (27) and Eq. (28)] improves the robustness at the zeros.

The critical parameter in the wide band technique is δR. δR controls the maximum value of the error scaling terms $a_n(\omega)$ and $b_n(\omega)$, as we will now show. When either kR_1 or kR_2 is a zero of the Bessel function, approximation error simplifies to the narrow band expression in Eq. (20). In the case $J_n(kR_1)=0$, the error scaling terms reduce to $a_n(\omega)=0$ and $b_n(\omega)=1/|J_n(kR_2)|$. For δR small, $J_n(kR_2)$ is also small and the linear approximation $J_n(kR_2)=k\,\delta R J_n'(kR_1)$ can be made. By the derivative property of the Bessel function $xJ_n'(x)=nJ_n(x)-xJ_{n+1}(x)$, we see that $J_n'(kR_1)=J_{n+1}(kR_1)$, so the nonzero error scaling term is

$$b_n(\omega)\approx\frac{1}{k\,\delta R|J_{n+1}(kR_1)|}.$$

From this equation, it seems advantageous to choose δR large, as a larger δR implies a smaller error scaling. However, δR cannot be too large, otherwise $J_n(kR_2)$ may coincide with another zero of the same Bessel function. As these Bessel functions are regularly spaced, we can select δR to avoid this case. From Eq. (24) the Bessel zeros of $J_n(kR)$ are spaced π apart, so set $k\,\delta R<\pi/2$ or $\delta R<\lambda/4$. An appropriate choice of δR is hence 1/4 of the smallest acoustic wavelength of interest.

C. Impact of measurement noise

In real rooms with background noise and sensor noise, it is nontrivial to obtain clean measurements of the acoustical

transfer functions. In this section we study how such noise impacts measurement of the sound field coefficients.

Model the measurement noise $\eta(\mathbf{x};\omega)$ at each sensor position $\mathbf{x}$ as additive white noise of zero mean and variance $\sigma^2(\omega)$. The noisy pressure is

$$\tilde{P}(\mathbf{x};\omega) = P(\mathbf{x};\omega) + \eta(\mathbf{x};\omega). \tag{30}$$

Calculating the DFT of both sides of Eq. (30) and comparing with Eq. (18), the noisy sound field coefficient estimates $\tilde{\beta}_n(\omega)$ are shown to be related to the noiseless estimates $\hat{\beta}_n(\omega)$ by

$$\tilde{\beta}_n(\omega) = \hat{\beta}_n(\omega) + \frac{1}{J_n(kR)} \mathrm{DFT}\{\eta(R,\phi_m;\omega)\}(n).$$

Inserting the definition of the DFT in Eq. (19) and rearranging:

$$\tilde{\beta}_n(\omega) - \hat{\beta}_n(\omega) = \frac{1}{J_n(kR)} \frac{1}{M} \sum_{m=0}^{M-1} \eta(R,\phi_m;\omega) e^{-i(2\pi mn/M)}. \tag{31}$$

Equation (31) is used to derive the mean and variance of the noisy sound field coefficient estimates. Taking the expectation of both sides of Eq. (31), the zero mean property of $\eta(R,\phi_m;\omega)$ implies that

$$E\{\tilde{\beta}_n(\omega) - \hat{\beta}_n(\omega)\} = 0,$$

or $E\{\tilde{\beta}_n(\omega)\} = \hat{\beta}_n(\omega)$. Measurement of the sound field coefficients remains unbiased by noise with zero mean. Multiplying Eq. (31) by its complex conjugate and taking the expectation, the variance is given by

$$\begin{aligned} E\{|\tilde{\beta}_n(\omega) - \hat{\beta}_n(\omega)|^2\} = {} & \frac{1}{[J_n(kR)]^2} \frac{1}{M^2} \\ & \times \sum_{m_1=0}^{M-1} \sum_{m_2=0}^{M-1} E\{\eta^*(R,\phi_{m_1};\omega) \\ & \times \eta(R,\phi_{m_2};\omega)\} \\ & \times \exp\{i2\pi(m_1 - m_2)n/M\}. \end{aligned}$$

In the case that noise is spatially uncorrelated, $E\{\eta^*(R,\phi_{m_1};\omega)\,\eta(R,\phi_{m_2};\omega)\} = \sigma^2(\omega)\,\delta_{m_1 m_2}$, and the variance reduces to

$$E\{|\tilde{\beta}_n(\omega) - \hat{\beta}_n(\omega)|^2\} = \frac{1}{M} \frac{\sigma^2(\omega)}{J_n(kR)^2}.$$

The variance is influenced by error scaling factor $1/|J_n(kR)|$. In the wide band case, we can use a similar derivation to show that the sound field coefficient estimates are also unbiased and have a variance given by

$$E\{|\tilde{\beta}_n(\omega) - \hat{\beta}_n(\omega)|^2\} = \frac{1}{M} \frac{\sigma^2(\omega)}{[J_n(kR_1)]^2 + [J_n(kR_2)]^2}. \tag{32}$$

The Bessel functions in the denominators of Eq. (32) show that similar error scaling occurs in the noise error of the wide band case.

This error scaling of the measurement noise impacts the measurability of the sound field coefficients. In general, when $J_n(kR)$ is small the error scaling causes a large amplification of measurement noise. For the inactive basis functions, the Bessel terms $J_n(kR)$ are so small as to be effectively zero. The resulting error scaling is so large that the sound field coefficients are unmeasurable, even for a small $\sigma^2(\omega)$.

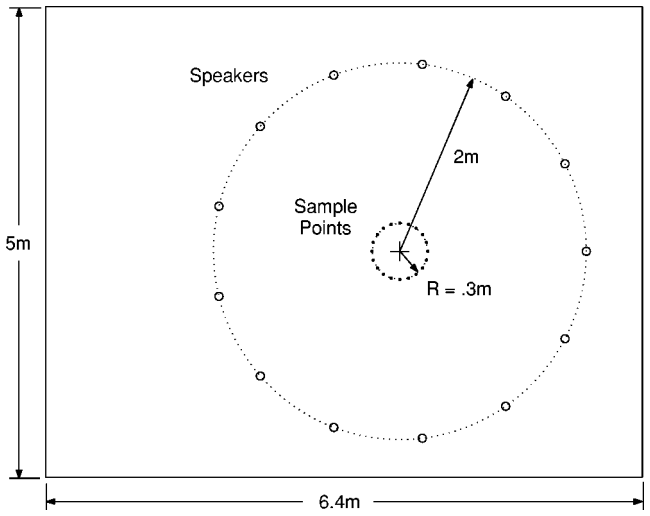

FIG. 6. Layout of loudspeakers (○) and pressure sample points (●) for sound field reproduction in the simulations. Though loudspeakers could be arbitrarily placed, we set them on a circle of radius 2 m centered about [3.8 m, 2.4 m].

IV. SIMULATION EXAMPLES

In the following examples, we illustrate the sound reproduction of a plane wave and a single monopole source at a single frequency (Sec. IV A and Sec. IV B) and at a range of frequencies (Sec. III D). Single frequency reproduction is performed at 1 kHz. Then in Sec. IV C we examine the performance of reproduction for the case that the numbers of loudspeakers are inadequate. In Sec. IV D we demonstrate the influence of measurement noise on reproduction error.

The reverberant room parameters and loudspeaker placement are summarized in Fig. 6. The room is rectangular with a wall absorption coefficient of 0.3 Unless otherwise stated, the control region has a radius of 0.3 m. Though the sound field reproduction design technique is applicable for any configuration and type of loudspeaker, we perform the sound field reproduction with a circular array of omnidirectional loudspeakers. This setup yields an average direct-to-reverberant energy ratio from each loudspeaker of -4.4 dB at the center of $\mathbb{B}^2$.

The loudspeaker requirements of this scenario are governed by the control region parameter $N = \lceil kR \rceil = 6$, prompting the use of $2N+1 = 13$ loudspeakers. Following the conservative design procedure of Sec. IV A with $\epsilon = -20$ dB, the maximum error scaling is $\kappa = 25$ dB, and from Fig. 4 the $\lceil \Delta N \rceil$ corresponding to $\kappa' = \epsilon/\kappa$ is 14. We hence sample the pressure at $M = N + \lceil \Delta N \rceil = 20$ points to measure the room response coefficients $\alpha_n(l,\omega)$.

The reverberation is generated with a 2-D adaptation of

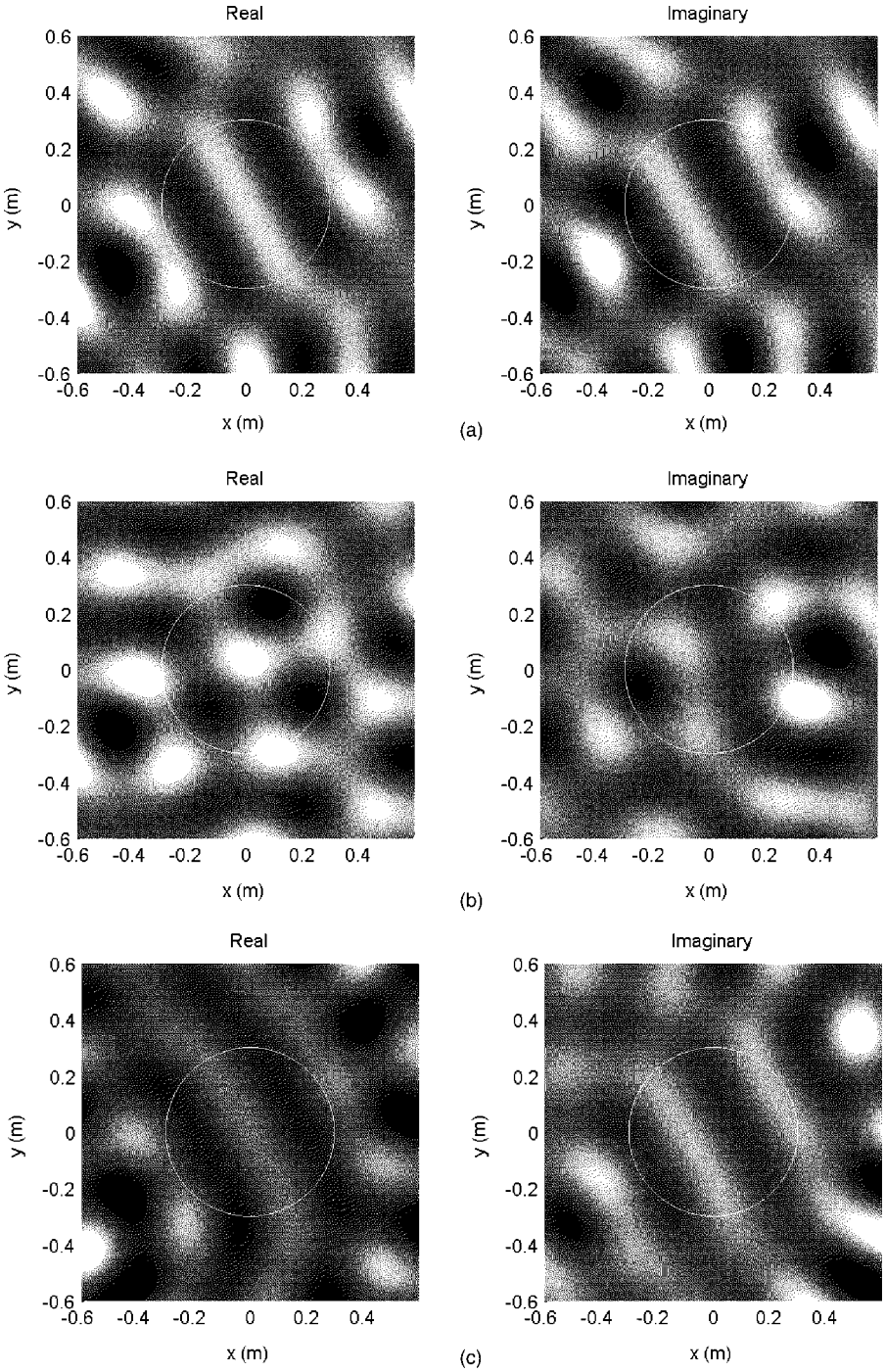

FIG. 7. The reproduction of a plane wave with 13 speakers and 20 pressure samples in a 0.3 m radius circle, for (a) a free field, (b) the same free field design in the reverberant room, and (c) a reverberant field design in the reverberant room. Reproduction errors are 0.87%, 307%, and 0.85%, respectively.

the image-source method.[19] Each of the room frequency response functions is given by

$$H(\mathbf{x};\omega)=\mathcal{H}_0^{(2)}(k\|\mathbf{x}-\mathbf{y}\|)+\sum_{n=1}^{N_i}\zeta_n\mathcal{H}_0^{(2)}(k\|\mathbf{x}-\mathbf{y}_n\|),$$

where $\mathcal{H}_0^{(2)}(\cdot)$ is the zeroth-order Hankel function of the second kind, $\mathbf{y}$ is the source position, and ζ_n and $\mathbf{y}_n$ are the position and accumulated reflection coefficient of the nth image-source, respectively. [For the 2-D point source, or a cylindrical source, $\mathcal{H}_0^{(2)}(kr)$ gives the field at a distance r from the source;[20] for a 3-D point source, this is equal to the more familiar expression $h_0^{(2)}(kr)=ie^{-ikr}/kr$.] Image-source positions are obtained through the repeated mirroring about the walls of the enclosure.[19] In simulations below, all the image-sources of up to fifth order were included (totaling $N_i=60$ image sources).

Sound field reproduction results are illustrated in Figs. 7–9. Here the real and imaginary parts of the complex pressure of the reproduced field are displayed as density plots. Details of the sound field reproduction in each case are described below.

A. Reproduction of a plane wave

First, the field pressure of a plane wave is reproduced. For a plane wave originating from direction $\hat{\mathbf{y}}$:

$$P_d(x;\omega)=e^{-ik\mathbf{x}\cdot\hat{\mathbf{y}}}.$$

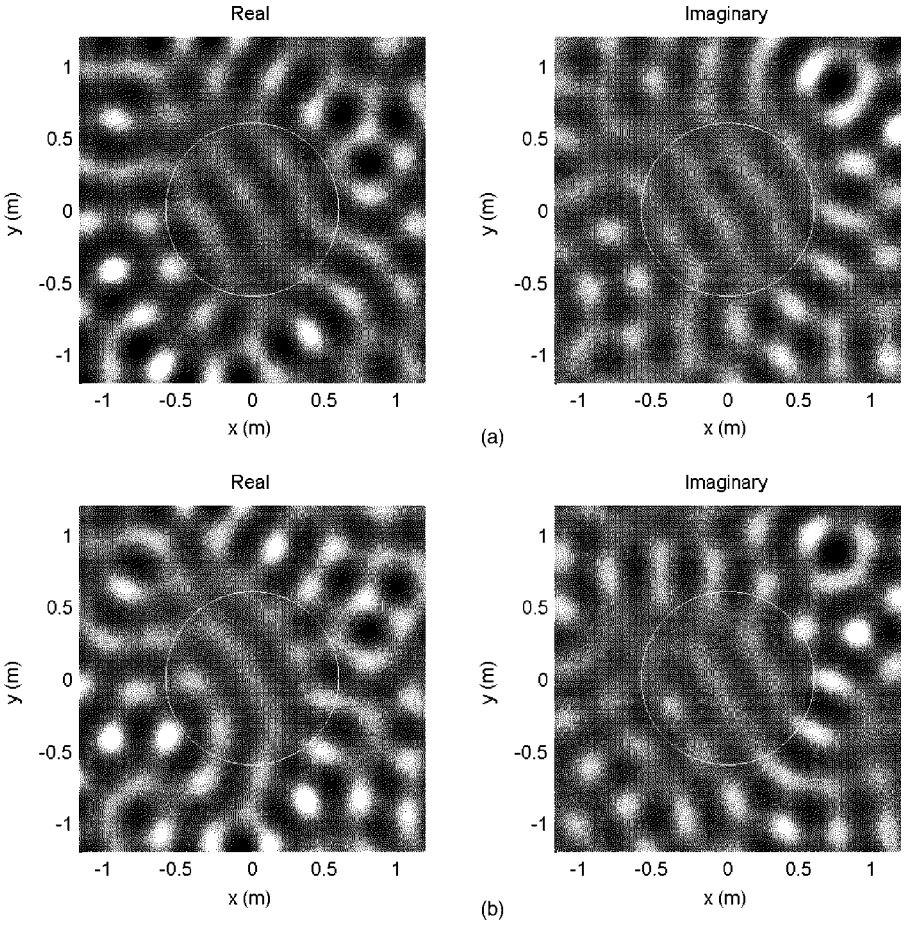

FIG. 8. The reproduction of a monopole in a 0.3 m radius circle of the reverberant room with 13 speakers and 20 pressure samples. The reproduction error is 2.12%. The position of the monopole is marked with a "+."

Through the Jacobi–Anger expression,[20]

$$e^{-ik\mathbf{x}\cdot\hat{\mathbf{y}}} = \sum_{n=-\infty}^{\infty} (-i)^n e^{-in\phi_y} J_n(kx) e^{in\phi_x},$$

where ϕ_y is the polar angle of $\hat{\mathbf{y}}$, one sees that the sound field coefficients are given by

$$\beta_n^{(d)}(\omega) = (-i)^n e^{-in\phi_y}.$$

Loudspeaker filter weights are chosen using the least squares approach of Sec. IV D.

Figure 7 illustrates the reproduction of a plane wave approaching from an angle of $\phi_y = \pi/6$. We provide a free field design [Fig. 7(a)], the same free field design in the reverberant room described above [Fig. 7(b)], and the reverberant field design [Fig. 7(c)]. With a 307% reproduction error, the reverberant performance of the free-field design is poor. In contrast, the reverberant design performs as well under such conditions as the free-field design does in a free field. Since the -4.4 dB direct-to-reverberant ratio here is common in room environments, we see the importance of reverberant field design techniques.

B. Reproduction of a phantom monopole source

The pressure field of a 2-D monopole source of unit strength is now reproduced. For a monopole source positioned at $\mathbf{y}$, the sound pressure is

$$P_d(x;\omega) = \mathcal{H}_0^{(2)}(k\|\mathbf{x}-\mathbf{y}\|).$$

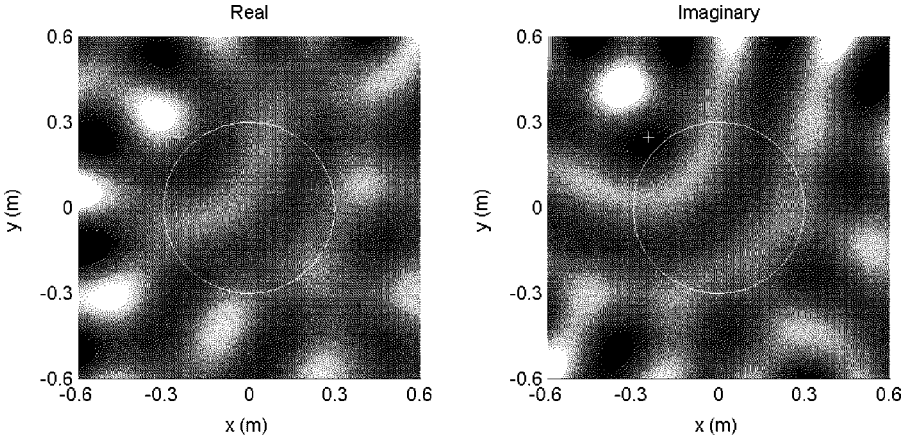

FIG. 9. The reproduction of a plane wave in a 0.6 m radius circle of the reverberant room with 13 speakers and 35 pressure samples when designed over (a) the whole region and (b) a region of 0.3 m radius. Reproduction errors are 26.0% and 84.1%, respectively.

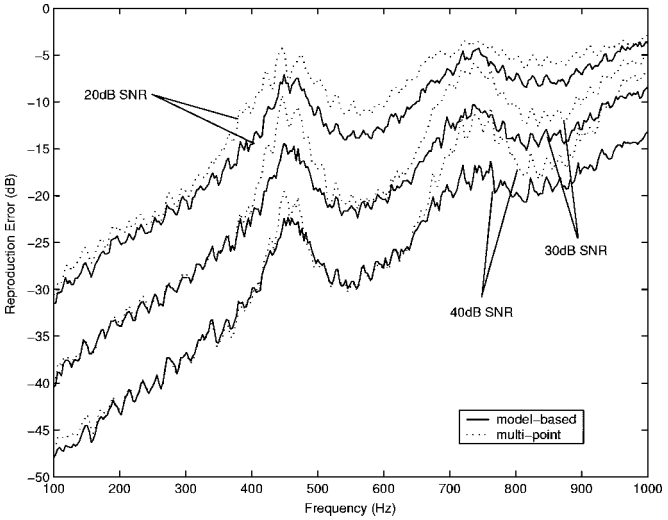

FIG. 10. Wide band reproduction of a plane wave in a 0.3 m radius circle with 13 speakers and using 40 pressure samples, using the model-based method (solid lines) and multiple-point method (broken lines). Reproduction error curves have been averaged over 40 trial runs.

Through the addition property of the Hankel function,[20]

$$\mathcal{H}_0^{(2)}(k\|\mathbf{x}-\mathbf{y}\|)=\sum_{n=-\infty}^{\infty}\mathcal{H}_n^{(2)}(ky)e^{-in\phi_y}J_n(kx)e^{in\phi_x},$$

where $y\triangleq\|\mathbf{y}\|$, one sees that the sound field coefficients are given by

$$\beta_n^{(d)}(\omega)=\mathcal{H}_n^{(2)}(ky)e^{-in\phi_y}.$$

Using the same design technique as for the plane wave reproduction, we simulate the reproduction of a monopole source just outside the region of interest, at $(y,\phi_y)=(0.35\,\mathrm{m},3\pi/4)$. Figure 8 shows a good reproduction of this monopole source.

C. Reproduction with an inadequate numbers of speakers

We now illustrate the result of designs with insufficient numbers of speakers. Again a plane wave is reproduced with 13 speakers, but over a region of interest of radius 0.6 m. At this radius, 25 basis functions are active. For comparison, we show the design for a radius of 0.3 m, where only the 13 lowest-order basis functions are reproduced. Because of the larger radius, we require more pressure samples (35 samples) for these designs.

The resulting sound fields are shown in Fig. 9. While the 0.3 m design reproduces accurately over where the 13 lowest-order basis functions are active [Fig. 9(b)], the 0.6 m design reproduces the sound field with better accuracy over the whole region of interest [Fig. 9(a)].

D. Wide band reproduction with measurement noise

Wide band sound field reproduction of a plane wave is performed with noisy pressure samples in the frequency range 100 Hz to 1 kHz, $R_1=0.3\,\mathrm{m}$, and $R_2=0.27\,\mathrm{m}$. The reproduction error is plotted in Fig. 10 for several noise SNRs averaged over 40 trial runs. This figure shows that at least 30 dB SNR is required for an accurate reproduction over the whole frequency range.

For comparison the multiple-point method has been co-plotted. As can be seen, the model-based method, by performing the least squares design over the whole region of interest, consistently outperforms the multiple-point method, typically up to 5 dB.

The general trend in this curve is that error increases with frequency. This trend is due to the linear increase in demand for loudspeakers and sensors with frequency. Our design uses the same number of loudspeakers and pressure samples for all frequencies. If we desire to flatten the curve, we could use less pressure samples and loudspeakers at lower frequencies where less basis functions are active.

Also observe the peaks in Fig. 10. These peaks occur in the vicinity of the zeros of the Bessel functions $J_0(kR)$ and $J_1(kR)$. Zeros of these Bessel functions at 460 and 730 Hz, respectively. These peaks are hence a direct result of the error scaling mentioned in Sec. IV C. To flatten such peaks, more pressure sampling should be performed about these frequencies, or the sensor pairs further separated (i.e., $\delta R=R_1-R_2$ should be increased).

V. CONCLUSION

We have described a novel method of performing sound field reproduction in reverberant enclosures. The key to this method is an efficient parametrization of the acoustical transfer functions. Using this parametrization, we have outlined a practical technique to precisely measure the acoustical transfer functions from a loudspeaker to each point in the region of sound reproduction. This approach allows full sound reproduction without prior knowledge of the loudspeaker positions nor the transmission characteristics of each loudspeaker. Through simulation, the reverberant field method is shown to perform as well in a reverberant room as free-field techniques do in a free field, and up to 5 dB better than multipoint least squares designs. The practical implementation of this soundfield reproduction scheme and its subjective performance remain as open questions and shall be addressed in future research.

APPENDIX A: PROOF OF EQ. (20)

Substituting Eq. (19) into Eq. (18) yields

$$\hat{\beta}_n(\omega)=\frac{1}{J_n(kR)}\frac{1}{M}\sum_{m=0}^{M-1}P(R,\phi_m;\omega)e^{-i(2\pi mn/M)},\tag{A1}$$

where $\phi_m=2\pi m/M$. Evaluating the basis function expansion of the sound field Eq. (16) at the M points (R,ϕ_m):

$$P\left(R,\frac{2\pi m}{M};\omega\right)=\sum_{q=-\infty}^{\infty}\beta_q(\omega)J_q(kR)e^{i(2\pi mq/M)}.\tag{A2}$$

Substituting Eq. (A2) into Eq. (A1) and interchanging summations:

$$\hat{\beta}_n(\omega)=\frac{1}{J_n(kR)}\frac{1}{M}\sum_{q=-\infty}^{\infty}\beta_q(\omega)J_q(kR)\sum_{m=0}^{M-1}e^{i[2\pi m(q-n)]/M}.$$

Now the summation of the complex exponential is given by

$$\sum_{m=0}^{M-1} e^{i[2\pi m(q-n)]/M} = \begin{cases} M, & \text{if } q-n|M, \\ 0, & \text{otherwise.} \end{cases}$$

Hence

$$\hat{\beta}_n(\omega) = \frac{1}{J_n(kR)} \sum_{s=-\infty}^{\infty} \beta_{n+sM}(\omega) J_{n+sM}(kR).$$

Rearranging,

$$\hat{\beta}_n(\omega) - \beta_n(\omega) = \frac{1}{J_n(kR)} \sum_{s=-\infty, \neq 0}^{\infty} \beta_{n+sM}(\omega) \times J_{n+sM}(kR).$$

QED.

APPENDIX B: BOUND ON THE TERMWISE SCALING FACTOR κ_n

For the following discussion, we view $J_n(kR)$ as a function of its order n. For $n \geqslant N = \lceil kR \rceil$, $J_n(kR)$ is observed to be a monotone decreasing function in n, decaying exponentially toward zero. (This property can be observed in Fig. 5 for n up to 20.) Similarly for $n \geqslant N$, $|J_{-n}(kR)|$ is also monotone decreasing in n.

From Eq. (21), the largest termwise scaling factor for coefficient $\hat{\beta}(\omega)$ is

$$\kappa_n = \frac{1}{J_n(kR)} \max_{q=-\infty,\ldots,\infty, \neq 0} |J_{n+qM}(kR)|.$$

Now since $M > 2N$, for $n = -N, -N+1, \ldots, N$ and $q = \pm 1, \pm 2, \ldots$, we have $|n+qM| > N$. Each of these Bessel functions $J_{n+qM}(kR)$ is hence sampled over the above-mentioned monotone decreasing interval. Consequently, κ_n is maximized when $|n+qM|$ is minimized:

$$\kappa_n = \begin{cases} J_{-(M-n)}(kR)/J_n(kR), & n \geqslant 0, \\ J_{M+n}(kR)/J_n(kR), & n < 0. \end{cases}$$

Calculating now the maximum κ_n over the active basis functions of positive index, the termwise scaling factor is bounded by

$$\max_{n=0,\ldots,N} \kappa_n = \max_{n=0,\ldots,N} \left| \frac{J_{-(M-n)}(kR)}{J_n(kR)} \right| \leqslant \max_{n=0,\ldots,N} 1/|J_n(kR)| \times \max_{n=0,\ldots,N} |J_{-(M-n)}(kR)|.$$

Again, due to the monotone decreasing property of the Bessel function:

$$\max_{n=0,\ldots,N} \kappa_n = \max_{n=0,\ldots,N} 1/|J_n(kR)| \times |J_{-(M-N)}(kR)|.$$

Similarly, due to the Bessel function property $J_{-n}(x) = (-1)^n J_n(x)$, the bound is the same for $\max_{n=-N,\ldots,-1} \kappa_n$. Then applying the Bessel function bound from Ref. 18,

$$\max_{n=-N,\ldots,N} \kappa_n = \max_{n=0,\ldots,N} 1/|J_n(kR)| \times \frac{1}{\sqrt{2\pi(M-N)}} \left[\frac{ekR}{2(M-N)} \right]^{M-N}.$$

QED.

[1] M. A. Gerzon, "Ambisonics in multichannel broadcasting and video," J. Audio Eng. Soc. **33**, 859–871 (1985).
[2] R. Nicol and M. Emerit, "3d-sound reproduction over an extensive listening area: a hybrid method derived from holophony and ambisonic," in *AES 16th International Conference on Spatial Sound Reproduction*, Helsinki, 1999, Vol. II, pp. 436–453.
[3] M. A. Poletti, "A unified theory of horizontal holographic sound systems," J. Audio Eng. Soc. **48**, 1155–1162 (2000).
[4] A. J. Berkout, D. D. Vries, and P. Vogel, "Acoustic control by wave field synthesis," J. Acoust. Soc. Am. **93**, 2764–2778 (1993).
[5] S. Takane, Y. Suzuki, and T. Sone, "A new method for global sound field reproduction based on Kirchhoff's integral equation," Acustica **85**, 250–257 (1999).
[6] S. Ise, "A principle of sound field control based on the Kirchoff–Helmholtz integral equation and the theory of inverse systems," Acustica **85**, 78–87 (1999).
[7] O. Kirkeby and P. A. Nelson, "Reproduction of plane wave sound fields," J. Acoust. Soc. Am. **94**, 2992–3000 (1993).
[8] O. Kirkeby, P. A. Nelson, F. Orduna-Bustamante, and H. Hamada, "Local sound field reproduction using digital signal processing," J. Acoust. Soc. Am. **100**, 1584–1593 (1996).
[9] D. B. Ward and T. A. Abhayapala, "Reproduction of a plane-wave sound field using an array of loudspeakers," IEEE Trans. Speech Audio Process. **9**, 697–707 (2001).
[10] J. Mourjopoulos, "On the variation and invertibility of room impulse response functions," J. Sound Vib. **102**, 217–228 (1985).
[11] P. A. Nelson and F. Orduna-Bustamante, "Inverse filter design and equalization zones in multichannel sound reproduction," IEEE Trans. Speech Audio Process. **3**, 185–192 (1995).
[12] O. Kirkeby and P. A. Nelson, "Digital filter design for inversion problems in sound reproduction," J. Audio Eng. Soc. **47**, 583–595 (1999).
[13] J. Mourjopoulos, "Digital equalization of room acoustics," J. Audio Eng. Soc. **42**, 884–900 (1994).
[14] S. Bharitkar and C. Kyriakakis, "A cluster centroid method for room response equalization at multiple locations," in *Proceedings of the IEEE Workshop on the Applications of Signal Processing to Audio and Acoustics*, Mohonk, 2001.
[15] F. Asano and D. C. Swason, "Sound equalization in enclosures using modal reconstruction," J. Acoust. Soc. Am. **98**, 2062–2069 (1995).
[16] A. O. Santillan, "Spatially extended sound equalization in rectangular rooms," J. Acoust. Soc. Am. **110**, 1989–1997 (2001).
[17] E. G. Williams, *Fourier Acoustics* (Academic, London, 1999).
[18] H. M. Jones, R. A. Kennedy, and T. D. Abhayapala, "On dimensionality of multipath fields: spatial extent and richness," in *Proceedings of the IEEE International Conference on Acoustics, Speech and Signal Processing*, Orlando, 2002, Vol. III, pp. 2837–2840.
[19] J. B. Allen and D. A. Berkley, "Image method for efficiently simulating small-room acoustics," J. Acoust. Soc. Am. **65**, 943–950 (1979).
[20] D. Colton and R. Kress, *Inverse Acoustic and Electromagnetic Scattering Theory* (Springer-Verlag, Berlin, 1992).